Spatial Channels for Wireless Over-the-Air Measurements in Reverberation Chambers*

Maria G. Becker[1], Robert D. Horansky[1], Damir Senic[1], Vincent Neylon[1], Kate A. Remley[1]
[1]RF Technology Division, National Institute of Standards and Technology, Boulder CO, USA, maria.becker@nist.gov

***Abstract*—NIST is developing a hybrid test chamber for over-the-air characterization of the next generation of wireless devices in spatial channel environments. By combining features of both reverberation and anechoic chambers, the hybrid chamber will produce anisotropic, multipath environments intended to test spatial diversity and beamforming capabilities of multiple-element antenna. Here, we present results that investigate our ability to control spatial channels. Synthetic-aperture measurements are used to determine the channel's power-angle profile and power-delay-angle profile, which characterize the angle-of-arrival and time-of-arrival of received power. Comparisons are made between an unloaded and loaded chamber. For the loaded configuration, strategically placed RF absorber is shown to create an anisotropic, spatial channel. The hybrid chamber is expected to provide a cost-effective solution for over-the-air measurements of next-generation wireless devices.**

***Index Terms*—Millimeter-wave metrology, power-angle profile, power-delay-angle profile, synthetic-aperture measurement, reverberation chamber, wireless system.**

I. Introduction

The widespread use of data-intensive smartphones, tablets, and other wireless devices is placing growing demands on communication channels. As a solution to this so-called spectrum crunch, a new generation of communication technology (5G) is being developed to operate at millimeter-wave frequencies [1,2]. The use of beamforming and spatial diversity requires multiple-element antenna systems that transmit and receive along directional, spatially-independent channels. The metrology infrastructure for telecommunications in directional-channel environments and at millimeter-wave frequencies is, however, incomplete. In response to the need for over-the-air (OTA) characterization procedures for the next generation of integrated wireless devices, we are developing a hybrid chamber that will combine reverberation and anechoic properties to produce controllable, spatial-channel testing environments. Contrary to conventional applications of reverberation chambers in OTA measurements where performance metrics are based on statistically isotropic channels [3-8], this innovative measurement technique will use reverberation chambers to produce highly anisotropic spatial channels with known, repeatable test conditions.

The hybrid chamber concept involves heavily loading a reverberation chamber with the intended goal of producing a static, anisotropic, multipath environment. The spatial and temporal properties of the channel produced inside the chamber are evaluated by means of a synthetic-aperture measurement, as described in [9]. The calculated power-angle profile provides a measure of the received power as a function of angle-of-arrival, while the power-delay-angle profile provides the instantaneous distribution of received power as a function of arrival time and angle-of-arrival.

As a preliminary step in developing a hybrid chamber for use at millimeter-wave frequencies, we have conducted a proof-of-concept study at microwave frequencies in a comparison of two chamber configurations, unloaded and loaded. In the loaded configuration, RF absorber covered a significant portion of one wall of the chamber (Fig. 1), while the rest of the chamber was free of absorber. The azimuthal angle-of-arrival is evaluated in terms of a power-angle profile for each chamber configuration. The presence of absorber creates an anisotropic channel that is qualitatively predictable. This suggests that we will be capable of reproducing specific spatial channel models in the hybrid chamber. The arrival times of the reflected signals (multipath components) are also evaluated in power-delay-angle profiles.

We begin in Section II by describing the 2-D synthetic-aperture measurements used to sample the chamber's wireless channel as a function of frequency and position. In Section III, we present a power-angle-profile analysis for each chamber configuration. The corresponding power-delay-angle profile analysis follows in Section IV. Concluding remarks and a discussion of the future outlook for the hybrid chamber are presented in Section V.

II. Synthetic-Aperture Measurements

Synthetic-aperture measurements have been used to study the spatial characteristics of static wireless channels [10,11], including those in reverberation chambers [9,12-15]. The latter work, which forms the basis of our analysis, involved measurement that scan an antenna through discrete locations on a two-dimensional spatial grid, creating a synthetic aperture in the azimuthal plane.

The measurement setup is illustrated in Fig. 1(a). The interior dimensions of the reverberation chamber are 1.875 m × 1.28 m × 1.76 m. Wall (0.88 m × 0.30 m) and ceiling (0.97 m × 0.40 m) paddles have travel distances of 1.4 m and 1.3 m, respectively. A vertically-polarized discone antenna functioned as the receive antenna, which was scanned across a horizontal synthetic-aperture grid; we used a 2-D positioning

* Work supported by U.S. government, not protected by U.S. copyright.

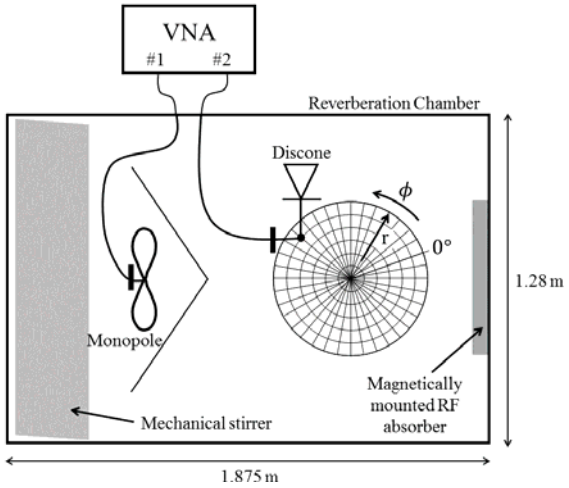

(a)

(b)

Fig. 1. Experimental setup for synthetic-aperture measurements: (a) top-down diagram and (b) photograph of chamber with loaded wall at left.

system, which consisted of an automated turntable and radial translation stage. The vertical position of the antenna within the chamber was 0.70 m above the floor and 0.42 m above the turntable platform. For each turntable position, the radial translation stage stepped through multiple positions, starting at the center of the turntable and ending at its outer diameter. In Fig. 1(b), the radial translation stage is positioned at its outermost position. The sample points of the synthetic aperture are the intersection points of concentric circles corresponding to different radii and radial lines corresponding to different turntable positions, as illustrated in Fig. 1(a). The angular resolution of the turntable is 84.5($\pm$0.1) μrad, and the linear resolution of the translation stage is 6.35($\pm$0.18) μm per manual specifications.

The transmit antenna was a polarization-balanced, double-sided, tapered, self-grounded monopole antenna [16]. It was positioned ~0.5 m above the floor and behind a metal shield to eliminate line-of-sight components of the channel [17]. Both unloaded and loaded chamber configurations were evaluated to investigate our ability to create directional channels. In the loaded configuration, a 60 cm × 90 cm section of a wall was covered with RF absorber, as shown in Fig. 1(b).

The transmit and receive antennas were connected to ports 1 and 2, respectively, of a calibrated vector network analyzer (VNA). The receive antenna was scanned across the 2-D grid at 36 angular steps of 10° and 7 radial steps of 4.5 cm, creating a circular synthetic-aperture with a diameter of 54 cm. Thus, the distance between adjacent grid points was less than $\lambda/2$ in accordance with the Nyquist criterion [10]. At each grid point and paddle orientation, complex S_{21} measurements were recorded from 1.8 to 2.2 GHz at 4001 uniformly spaced frequencies. The VNA's intermediate frequency (IF) bandwidth was 1 kHz and the dwell time was 10 μs. We recorded measurements at nine independent paddle configurations using three vertical and three horizontal paddle positions. To a first order, the S_{21} scattering parameter represents the wireless channel's transfer function $h^{(n)}(f, \boldsymbol{r})$, where f is frequency, $\mathbf{r} = (r, \theta)$ is the receive antenna position on the 2-D grid, and $n = 1 \ldots 9$ indicates paddle configuration. Including mismatch correction and antenna efficiency in the formulation is the subject of future work.

III. Power-Angle Profiles

To extract angle-of-arrival information from synthetic-aperture measurements of the channel's transfer function, we use Fourier analysis. The resulting power-angle profiles indicate the distribution of received power as a function of azimuthal arrival angle.

As described in [9], we obtain the 2-D power-wavevector profile $p^{(n)}(f, \mathbf{k})$ by taking the magnitude squared of the Fourier transform with respect to position of the channel transfer function for a particular frequency and paddle configuration:

$$p^{(n)}(f, \mathbf{k}) = \left| \int h^{(n)}(f, \mathbf{r}) e^{j\mathbf{k}\cdot\mathbf{r}} d\mathbf{r} \right|^2. \quad (1)$$

The 2-D wavevector is indicated by $\mathbf{k} = (k, \beta)$, where β is an outgoing angle. Prior to taking the Fourier transform in (1), we apply a 2-D Hamming window to the transfer function to minimize aperture sidelobes. Also, to simplify the analysis, we convert the channel transfer function, recorded in polar coordinates, to Cartesian coordinates prior to the Fourier transform. To achieve this, we interpolate the polar coordinate data onto a Cartesian grid with a step size that matches the largest step size of the polar grid. We calculate power-angle profiles by converting back to polar coordinates (k, β), again using an interpolation technique, and integrating over wavenumber, we get:

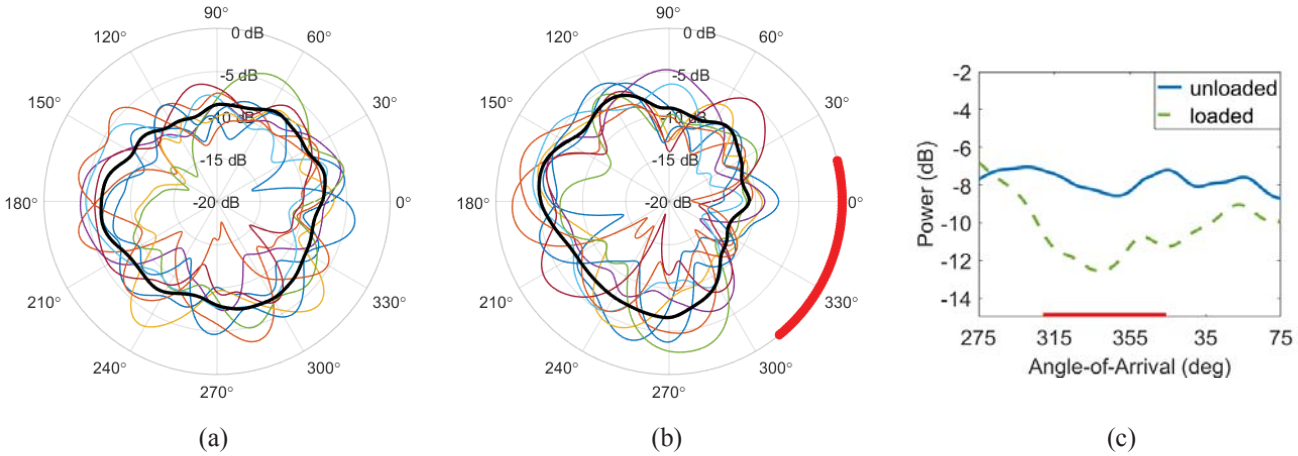

(a) (b) (c)

Fig. 2. Power-angle profiles at 2 GHz in the (a) unloaded and (b) loaded chamber. The nine, thin, colored profiles, each normalized to the total integrated received signal level, correspond to nine independent paddle positions; the thick, black trace corresponds to their average. The direction of the absorber is indicated in red on the angular axis at 0 dB for the loaded chamber. (c) The average power-angle profiles are plotted for angles spanning the placement of absorber; the difference is approximately 3-5 dB in the direction of the absorber, indicated in red.

$$p^{(n)}(f,\phi) = \int_0^{k_0} p^{(n)}(f,k,\beta+\pi)\,dk, \qquad (2)$$

where k_0 is the free-space wavenumber. This integration over wavenumber corresponds to an integration with respect to elevation angle, such that multipath components arriving from above and below the horizon are projected onto the azimuthal plane. The outgoing propagation angle β has been mapped to the incoming arrival angle ϕ with the addition of π.

Power-angle profiles for the loaded and unloaded configurations are shown in Figs. 2(a) and (b), respectively, for nine independent paddle configurations (thin lines), as well as their average (thick line). For the loaded case, the position of the RF absorber is also indicated (thick line at edge of polar plot). Each profile has been normalized to the total integrated signal level, such that an integral of a single profile with respect to the polar angle would give 0 dB. The result is a relative power based on $|S_{21}|^2$. The uncertainty in the angle ϕ is given by the turntable repeatability of 4.25 μrad.

As expected, the stirred, unloaded chamber produces an isotropic environment relative to the hybrid chamber, indicated by little variation in the mean power-angle profile (Fig. 2(a)) as a function of azimuth angle. Additional paddle stirring is expected to further increase the isotropicity. When the chamber wall is loaded, however, there is less power received from the direction of the loaded wall relative to other directions. On average, the power is reduced by approximately 3-5 dB in the direction of absorber, as indicated by Fig. 2(c). Thus, a directional channel has been created in the reverberation chamber.

The angular resolution of the synthetic-aperture measurements is limited by the diameter of the aperture. It can be approximated with the Rayleigh criterion [18]:

$$\sin\theta_R = 1.22\frac{\lambda}{D}, \qquad (3)$$

where λ is wavelength, D is the diameter of the aperture, and θ_R is the minimum resolvable angular beamwidth. Based on this criterion, our experimental setup ($D = 54$ cm, $\lambda = 15$ cm) is capable of resolving beamwidths down to 20° at 2 GHz. This estimate is consistent with the lobes in the power-angle profiles of Figs. 2(a) and 2(b). The long-term goal of this project is to create and characterize directional channel environments for millimeter-wave frequencies, where much higher angular resolution is desired. At 28 GHz, the same array diameter will provide 1.4° resolution, which is expected to meet the future demands of the wireless industry.

We note that antenna-environment multiple scattering effects could include perturbation of the channel by the receive antenna and its positioning system [14]. The error due to such effects was not studied in this initial investigation, but will be part of future work.

IV. Power-Delay-Angle Profiles

Fourier analysis can also be used to extract time-of-arrival information from synthetic-aperture measurements of the channel's transfer function. The resulting power-delay-angle profiles indicate the instantaneous distribution of received (relative) power as a function of arrival time τ, as well as azimuthal arrival angle ϕ. As described in [9], the 2-D power delay-wavevector profile $p^{(n)}(\tau,\mathbf{k})$ is obtained by taking the magnitude squared of the Fourier transform of the channel transfer function with respect to position and frequency for a particular paddle position:

$$p^{(n)}(\tau,\mathbf{k}) = \left|\iint h^{(n)}(f,\mathbf{r})e^{j2\pi\tau f}e^{j\mathbf{k}\cdot\mathbf{r}}df\,d\mathbf{r}\right|^2. \qquad (4)$$

To avoid sidelobes, a 1-D Hamming window is applied to the channel transfer function in the frequency dimension, in addition to the 2-D Hamming window in the spatial domain, prior to the Fourier transforms in (4). We arrive at the power-

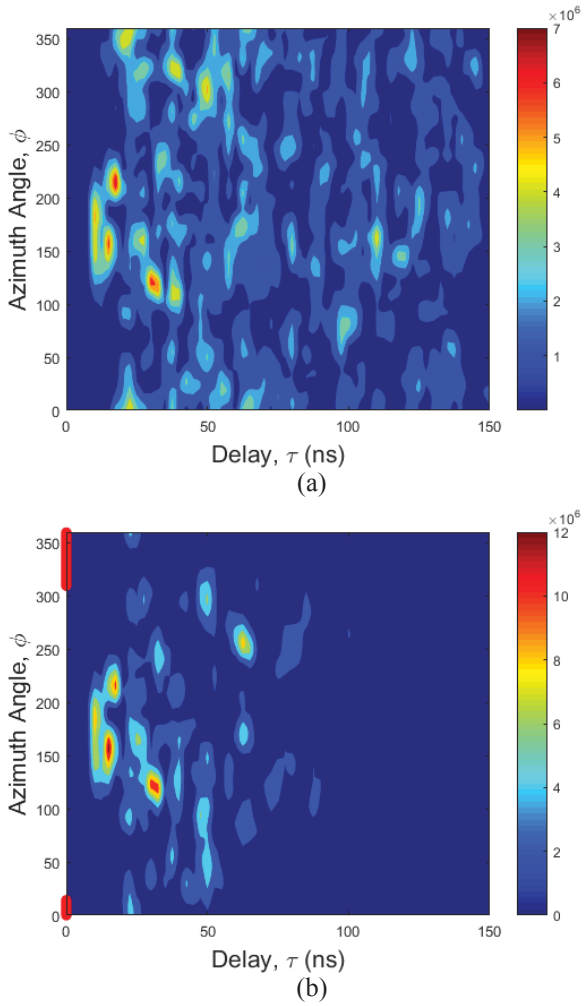

Fig. 3. Power-delay-angle profiles in the (a) unloaded and (b) loaded chamber for a single paddle position. Each profile is normalized to the total integrated signal.

delay-angle profile for a particular paddle position by integrating over wavenumber:

$$p^{(n)}(\tau,\phi) = \int p^{(n)}(\tau,k,\beta+\pi)dk. \qquad (5)$$

Power-delay angle profiles for the loaded and unloaded chamber configurations are shown in Fig. 3 for a single paddle orientation. For the loaded case, the angular position of the RF absorber is also indicated. Each profile has been normalized to the total integrated signal level such that integrating over delay and azimuth would result in unity. The time interval used in Figs. 3(a) and (b) is $\Delta t = 2.5$ ns and the angle interval is $\Delta\phi = \pi/360$. While the color scale for relative power values is given in linear units, the corresponding decibel values can be obtained by multiplying by the time and angle interval values given above, then taking the log and multiplying by ten.

As expected, less power is received at longer delay times for the loaded configuration, as compared to the unloaded configuration. The absence of power received from the direction of the loaded wall is also evident.

The temporal resolution of the power-delay-angle profile is determined from the bandwidth of frequencies used in the Fourier transform of (5) according to $\Delta t = 1/\Delta f$. The resulting temporal resolution from our 400 MHz bandwidth is 2.5 ns.

V. Conclusion

A hybrid chamber designed to create spatial channels that replicate millimeter-wave channel models is being developed at NIST for OTA characterization of next generation wireless devices. In a proof-of-concept study at microwave frequencies, we have demonstrated our ability to create a sample spatial channel environment with strategic placement of RF absorber. We characterized the spatial and temporal properties of the spatial channel in 2-D power-angle and power-delay-angle profiles using synthetic-aperture measurements. Ongoing work towards the development of the hybrid chamber will include extending the analysis to three dimensions. In our preliminary study, we measured vertically-polarized plane-waves. Future work will include analyzing spatial-channel environments for all three plane-wave polarizations. Accounting for mismatch correction, antenna efficiency, multiple scattering effects, and uncertainty will also be subjects of future work.

The hybrid chamber is expected to increase the flexibility of the reverberation chamber setup for testing wireless devices by emulating anisotropic, directional-channel environments. This cost-effective approach has the potential for high impact applications in the wireless industry where multiple-element antenna systems are being integrated in an increasing number of wireless devices, with the performance of each new model needing to be tested under directional-channel conditions prior to certification. Development of the hybrid chamber supports advanced wireless communication technology by providing necessary metrology infrastructure and standardized, measurement methods, ultimately with known uncertainties. The development of such technology is essential for meeting the expected increase in demand for wireless channel capacity.

References

[1] T. S. Rappaport, S. Sun, R. Mayzus, H. Zhao, Y. Azar, K., Wang, G. N. Wong, J. K. Schulz, M. Samimi, and F. Gutierrez, "Millimeter wave mobile communications for 5G cellular: It will work!" *IEEE Access*, vol. 1, pp. 335-349, May 2010.

[2] K. A. Remley, J. A. Gordon, D. Novotony, A. E. Curtin, C. L. Holloway, M. T. Simons, R. D. Horansky, M. S. Allman, D. Senic, M. Becker, J. A. Jargon, P. D. Hale, D. F. Williams, A. Feldman, J. Cheron, R. Chamberlin, C. Gentile, J. Senic, R. Sun, P. B. Papazian, J. Quimby, M. Mujumdar, and N. Golmie, "Measurement challenges for 5G and beyond," *IEEE Microwave Magazine*, pp. 41-56, July/Aug. 2017.

[3] P. D. Donker and R. Meys, "Statistical response of antennas under uncorrelated place wave spectrum illumination," *Electromagnetics*, vol. 24, no. 6, pp. 409-423, 2004.

[4] P.-S. Kildal and K. Rosengren, "Correlation and capacity of MIMO systems and mutual coupling, radiation efficiency, and diversity gain of their antennas: Simulations and measurements in a reverberation

chamber," *IEEE Commun. Mag.*, vol. 42, no. 2, pp. 104-112, Dec. 2004.

[5] K. Rosengren and P.-S. Kildal, "Radiation efficiency, correlation, diversity gain and capacity of a six-monopole antenna array for a MIMO system: Theory, simulation and measurement in reverberation chamber*," IEEE Proc.-Microw. Antennas Propag.*, vol. 152, no. 1, pp. 7-16, Feb. 2005.

[6] U. Carlberg, J. Carlsson, A. Hussain, and P.-S. Kildal, "Ray based multipath simulation tool for studying convergence and estimating ergodic capacity and diversity gain for antennas with given far-field functions, in *Proc. ICECom*, Dubrovnik, Croatia, Sep. 20-23, 2010, pp. 1-4.

[7] T. B. Hansen, "Correlation and capacity calculations with reference antennas in an isotropic environment," *Int. J. Antennas Propag*., vol. 2012, pp. 1-4, 2012.

[8] R. J. Pirkl and K. A. Remley, "MIMO channel capacity in 2-D and 3-D isotropic environments," *Int. J. Antennas Propag.*, vol. 2012, pp. 1-11, 2012.

[9] R. J. Pirkl and K. A. Remley, "Experimental evaluation of the statisitical isotropy of a reverberation chamber's plane-wave spectrum," *IEEE Trans. Electromagn. Compat.*, vol. 56, no. 3, pp. 498-509, June 2014.

[10] J. Fuhl, J.-P. Rossi, and E. Bonek, "High-resolution 3-D direction-of-arrival determination for urban mobile radio," *IEEE Trans. Antennas Propag.*, vol. 45, no. 4, pp. 672-682, Apr. 1997.

[11] J. Larila, K. Kalliola, M. Toeltsch, K. Hugl, P. Vainikainen, and E. Bonek, "Wide-band 3-D characterization of mobile radio channels in urban environment," *IEEE Trans. Antennas Propag.*, vol. 50, no. 2, pp. 233-343, Feb. 2002.

[12] R. J. Pirkl, "Spatial autocovariances os S-parameter measurements in a lossy reverberation chamber," *IEEE Trans. Electromagn. Compat.*, vol. 55, no. 4, pp. 671-682, Aug. 2013.

[13] R. J. Pirkl, J. M. Ladbury, and K. A. Remley, "The reverberation chamber's unstirred field: a validation of the image theory interpretation," in *Proc. Int. Symp. Electromagn. Compat.*, Long Beach, CA, USA, Aug. 14-19, 2011, pp. 670-675.

[14] R. J. Pirkl and K. A. Remley, "Antenna-environment multiple scattering in reverberation chambers," in *IEEE AP-S*, Spokane, WA, USA, Jul. 4-8, 2011, pp.1-4.

[15] A. A. Glazunov, S. Prasad, and P. Handel, "Experimental characterization of the propagation channel along a very long virtual array in a reverberation chamber," *Progress in Electromagnetics Research B*, vol. 59, pp.205-217, 2014.

[16] A. Al-Rawi, A. Hussain, J. Yank, M. Franzén, C. Orlenius, and A. Kishk, "A new compact wideband MIMO antenna- The double-sided tapered self-grounded monopole array," *IEEE Trans. Antennas Propag.*, vol. 62, no. 6, June 2014.

[17] P.-S. Kildal, X. Chen, C. Orlenius, M. Franzén, and C. S. Lötbäck Patané, "Characterization of reverberation chambers for OTA measurements of wireless devices: Physical formulations of channel matrix and new uncertainty formula," *IEEE Trans. Antennas Prpag.*, vol. 60, no. 8, Aug. 2012.

[18] E. Hecht and A. Zajac, Optics. Reading, MA, USA:Addison-Wesley Publishing, 1974, pp. 353-354.